

Design and demonstration of a low-field magnetic resonance imaging rhizotron for in-field imaging of energy sorghum roots

G. Cody Bagnall¹  | Stephen A. Altobelli² | Mark S. Conradi² | Hilary T. Fabich² | Eiichi Fukushima² | Neha Koonjoo⁴ | Dean O. Kuethe² | William L. Rooney¹  | Karl F. Stupic⁷ | Bragi Sveinsson⁴ | Brock Weers⁸ | Nithya Rajan¹  | Matthew S. Rosen^{4,5,6,#}  | Cristine L. S. Morgan^{3,#} 

¹Texas A&M AgriLife Reseach, 2147 TAMU, College Station, TX 77843, USA

²ABQMR Inc., 2301 Yale Blvd. SE, Suite C2, Albuquerque, NM, 87106, USA

³Soil Health Institute, 2803 Slater Road Suite 115, Morrisville, NC 27560, USA

⁴Athinoula A. Martinos Center for Biomedical Imaging, Dep. of Radiology, Massachusetts General Hospital, Charlestown, MA 02129, USA

⁵Harvard Medical School, Boston, MA 02115, USA

⁶Dep. of Physics, Harvard Univ., Cambridge, MA 02138, USA

⁷Applied Physics Division, National Institute of Standards and Technology, 325 Broadway, Boulder, CO 80305, USA

⁸Dep. of Biochemistry and Biophysics, Texas A&M Univ., College Station, TX, USA

Correspondence

G. Cody Bagnall, Texas A&M AgriLife Reseach, 2147 TAMU, College Station, TX 77843, USA.

Email: gcbagnall@outlook.com

Assigned to Associate Editor Daniel Northrup.

#These authors contributed equally.

Funding information

Advanced Research Projects Agency - Energy, Grant/Award Number: DE-AR0000823

Abstract

Root phenotyping provides critical information to plant breeders for developing varieties with improved drought tolerance, greater root biomass, and greater nutrient use efficiency. Phenotyping roots in the natural environment is important for understanding the effect of the soil environment on root genotypic expressions. The goal of this work was to design and test a field-scale mobile low-field magnetic resonance imaging (LF-MRI) Rhizotron that produces actionable root phenotyping data. We demonstrated this novel technology for root visualization and quantification using a LF-MRI Rhizotron operating at 47 mT with two soil types. The LF-MRI Rhizotron weighs 453 kg, with a height of 90 cm, a diameter of 28 cm and an imaging field of view of 28 cm × 28 cm. The unit was operated in a Belk clay (Entic Hapluderts) and Weswood silt loam (Udifluventic Halustepts) generating 2-D and 3-D image data sets. The 2-D image data had a collection time of 16.5 min per image at an image resolution of 2.2 mm per pixel. The 3-D data had a collection time of 13 h per image with a 2.2 × 2.2 × 2.2 mm voxel resolution. Low-field magnetic resonance imaging worked well for visualizing roots in moderate to high clay soils, demonstrating the

Abbreviations: CT, computed tomography; FOV, field of view; LF-MRI, low-field magnetic resonance imaging; MR, magnetic resonance; MRI, magnetic resonance imaging; NMR, nuclear magnetic resonance; RF, radio frequency; SNR, signal-to-noise ratio.

This is an open access article under the terms of the [Creative Commons Attribution-NonCommercial-NoDerivs](https://creativecommons.org/licenses/by-nc-nd/4.0/) License, which permits use and distribution in any medium, provided the original work is properly cited, the use is non-commercial and no modifications or adaptations are made.

© 2022 The Authors. *The Plant Phenome Journal* published by Wiley Periodicals LLC on behalf of American Society of Agronomy and Crop Science Society of America

potential for this technology; however, the broad application of this platform is hampered due to the prohibitively long scanning time to obtain 3-D images. By increasing the field strength, and therefore the signal-to-noise ratio, faster scan times can enable a more useful system for root phenotyping.

1 | INTRODUCTION

It is well established that root system architecture plays an important role in plant growth and productivity (Fenta et al., 2014; Henry et al., 2011; Kano-Nakata et al., 2019; Lopez-Bacio et al., 2003; Paez-Garcia et al., 2015; Wasaya et al., 2018). Soil conditions such as pH, temperature, and salinity affect root system architecture (Koevoets et al., 2016) and hence are important considerations in the plant breeding process. However, in situ nondestructive root measurements for the purpose of crop improvement are difficult, due to the opaque nature of soils. The process of measuring roots in natural soil is labor intensive and often requires digging root and washing away soil before measurements can be acquired. Characterizing root traits of crops growing in soil is important to generate crop phenotypes that have drought tolerance (Ayalew et al., 2015; Fenta et al., 2014), improved nutrient use efficiency (Garnett et al., 2009), and increased rooting depth and biomass for enhancing soil organic carbon storage (Paus-tian et al., 2016).

Root phenotyping can be subdivided into two categories: (a) greenhouse and/or growth chamber-based phenotyping and (b) field-based phenotyping. In greenhouses and growth chambers, the environment is highly controlled which permits the construction of meticulous experiments. However, replicating plant-to-plant interactions and other soil and environmental conditions such as light and temperature fluctuations, wind, soil structure, and soil heterogeneity are difficult to achieve in greenhouses and growth chambers. Greenhouse techniques for root phenotyping include growing plants in hydroponics (Ayalew et al., 2015), clear gel growth media (Ma et al., 2019), or aeroponics (Pingault et al., 2018) to study root structure. These systems allow roots to be measured and inspected more easily, but at the cost of not quantifying the effect of the natural soil environment on root growth. When natural soils are used in growth chamber and greenhouse experiments, the soil is often ground and packed into pots or rhizotrons. Packing dried and ground soil removes natural preferential pathways associated with soil structure and homogenizes soil porosity and texture, thus changing the rooting environment from those found in intact soils. Rhizotron edges also restrict root growth, resulting in edge effects at some point during the plant's growth.

In-field root phenotyping affords researchers the opportunity to investigate plant-to-plant interactions, soil-plant inter-

actions, and the effect of environmental factors and management practices on root growth. However, field-based root phenotyping has less sophisticated tools available for measuring root growth and architecture. A common field-based method is the excavation and washing of roots, also known as “shovelomics.” Typically, roots are either scored visually (Trachsel et al., 2011) or imaged on a processing platform to quantify root morphometrics (Bucksch et al., 2014; Grift et al., 2011). This method allows the quantification of many root traits, is low tech (high usability) and can be used for high throughput. Shovelomics, however is labor intensive and the true root system architecture cannot be known once the soil is removed, making it difficult to determine how much information is lost. Shovelomics tends to work well for core root metric information such as nodal root length or root crown size.

Other field-based methods include use of mini-rhizotrons (Iversen et al., 2012), electrical root capacitance (Chloupek, 1997; Messmer et al., 2011), and soil coring (Fenta et al., 2014; Wasson et al., 2014). The mini-rhizotron method provides information on timing and abundance of root growth but does not provide useful root architecture data because roots in this system tend to preferentially grow around rhizotron tubes. Electrical root capacitances can provide estimates of root biomass nondestructively, thus providing root biomass accumulation over time. Capacitance methods lack the ability to produce root length, diameter, or architectural information. Collecting soil and root cores allows root diameters to be correlated with depth and distances from the main stem but does not provide root architectural information or total root biomass accumulation over time since the plant is destroyed during sampling. In addition, working in soils containing high amounts of silicate clays is difficult because of the chemical and physical properties of silicate clays (Logsdon, 2009; Miller et al., 2002). Lack of advanced tools suitable for field-based root phenotyping is a significant impediment to root phenotyping in the field (Fenta et al., 2014). Therefore, root phenotyping technologies that can be operated in the field and can capture the interaction between genetics, environment, and management ($G \times E \times M$) are needed.

Various imaging systems such as 2-D optical scanners (Araujo et al., 2004) and X-ray computed tomography (CT) (Mairhofer et al., 2013; Mooney et al., 2012) have been used for root phenotyping. The 2-D optical scanners work well for small seedlings in a laboratory setting, but roots quickly run out of room as they develop. In addition, the system

requires that roots are pressed between two surfaces for imaging, resulting in relatively simple 2-D root structure. X-ray CT systems are effective at imaging root system architecture. However, these systems have difficulty segmenting roots from soil. In addition, safety and infrastructure requirements make these systems best suited for laboratory use only, at this juncture.

Magnetic resonance imaging (MRI) systems have been tested and used for both above and below ground plant phenotyping (Borisjuk et al., 2012; Fiorani & Schurr, 2013). High field MRI systems (ranging from 1 to 10 T) have been used to measure soil water relaxation times. Studies have found that different soil types have unique relaxation times, thus developing a universal calibration method is difficult (Hall et al., 1997; Metzner et al., 2015). High-field MRI has shown the ability to differentiate between soil water and root water (Rogers & Bottomley, 1987). However, magnetic material found in some soils tends to create significant distortions in the images when operating at high field, especially in soil with more than 10% clay content (Pflugfelder et al., 2017), or more than 4% paramagnetic material by weight (Dusschoten et al., 2016). High-field MRI systems are capable of creating high-quality 3-D root system architecture images and generate root phenotyping data (Gruwel, 2014; Hillnhutter et al., 2012; Metzner et al., 2015). However, due to the aforementioned soil constraints, coupled with high power demands and MRI sensitivity to environmental radio frequency (RF) noise, these systems are often overlooked for root imaging. Bagnall et al. (2020) showed that by using a low-field magnetic resonance imaging (LF-MRI), roots could be detected and visualized in high clay soils in a controlled environment. That work demonstrated the use of a LF-MRI system to mitigate the detrimental effects that magnetic material found in moderate and high clay soils have on MRI quality. This LF-MRI approach balanced the competing aspects of signal averaging, image resolution, and acquisition time to obtain images of good quality over practical acquisition times. Low-field MRI data collection has also been paired with a novel deep neural network method (AUTOMAP) to improve the quality of the reconstructed images (Koonjoo et al., 2021; Zhu et al., 2018). The LF-MRI system was prototyped and tested under laboratory conditions so it was unknown how well the equipment would function under field conditions and the impact that environmental electromagnetic noise could have on the data quality.

In this paper, we present the design, operation, and imaging results from a mobile field-deployable 47 mT (2 MHz Larmor frequency) MRI Rhizotron system. A truly field-based system must work in hot and humid environment of an agricultural field and work in natural soils. Using techniques from Bagnall et al. (2020), we demonstrated that the LF-MRI system was capable of collecting 2-D and 3-D root system architecture images under agricultural field conditions. We addressed this goal through the following specific objectives: (a) design and

Core Ideas

- The goal of this work was to develop and test a novel field-based root imaging system.
- This work is the first step in the development of a truly mobile in-ground field-based low-field-MRI system.
- Low-field MRI worked well for root imaging in high clay soils under field conditions.

construct a field deployable LF-MRI system and (b) demonstrate the use of LF-MRI system in an agricultural field for root image data collection.

2 | MATERIALS AND METHODS

2.1 | The LF-MRI field-deployable rhizotron system

The LF-MRI Rhizotron was designed to operate in the greenhouse or agricultural field under environmental conditions of high air temperature and humidity. These requirements placed an upper bound on the size and weight of the system. The ability to switch off the magnetic field if needed for safety while operating in a field informed the decision for building the LF-MRI Rhizotron platform around an electromagnet rather than a permanent magnet. The Rhizotron also needed to be large enough to capture a significant portion of the root system to be useful in root phenotyping. A cylinder with inner diameter and height of 25 cm (12.7 L) was a sufficient balance of these competing requirements.

A schematic of the field equipment layout of the LF-MRI Rhizotron system is shown in Figure 1. Field equipment included generators, an air-conditioned trailer, and other items to support the magnet and data acquisition. The trailer contained LF-MRI electronics and computing equipment and was powered by the two generators. The water chiller and oil pump worked in tandem to keep the LF-MRI electromagnet from overheating.

2.2 | Description of LF-MRI electromagnet

The in-field LF-MRI Rhizotron was comprised of both pre-fabricated and specially fabricated equipment. Because mobility was crucial for the LF-MRI Rhizotron, a $3.6 \times 1.5 \times 1.5$ m box trailer was used to keep sensitive equipment cool and protected from rain and dust. The trailer was outfitted with a heating and cooling unit and was

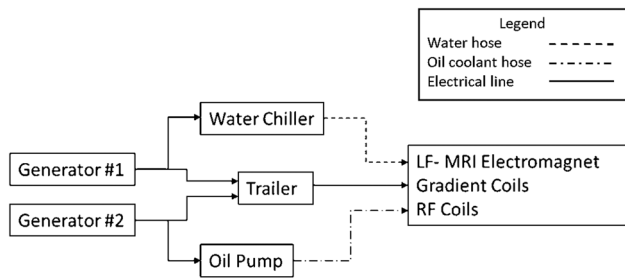


FIGURE 1 Schematic of the low-field magnetic resonance imaging (LF-MRI) Rhizotron equipment layout for field data collection. Two generators powered the trailer, water chiller, and oil pump. An air-conditioned trailer housed the LF-MRI control electronics, which is connected to the electromagnet. Solid lines denote electrical connections, the dotted line denotes a water line connection and the dot-dash-dot line an oil hose connection

wired with two electrical panels. Each panel was powered by a single 220V AC (alternating current) gasoline-powered generator (XP12000EH, Duromax). The generators were placed approximately 12 m away on the opposite side of the trailer from the electromagnet to reduce acoustic noise and minimize RF interference.

The electronic and computing equipment for the Rhizotron system included an MRI console (Redstone, Tecmag), which acted as a system controller for the LF-MRI Rhizotron. The console tower also housed the RF receiver, RF transmitter, and magnetic field gradient amplifiers. A separate power supply converted the AC voltage to DC voltage for operating the electromagnet system (Figure 2).

Three amplifiers (model 2105, AE Techron) with a 50 A, 45V max were operated at 10 A to drive the gradient coils (Figure 3a). An RF power amplifier (BT-0100 Alphas S-T, Tomco) (Figure 3b), which has a 1,000 W pulse max, was operated at a 200 W output used to operate the RF transmitter coils. Three switching power supplies (Model 6032A, Hewlett-Packard) were used to power the electromagnet. Interior LED lighting, a desktop computer, and an air-cooling system were also housed and operated inside the trailer.

The cooling system, magnet, gradient coils, and RF coil were located outside the trailer. The magnetic field was produced by an electromagnet with a solenoidal main coil and two end-correction coils, all of which were wound on a stainless steel bobbin (Figure 4). The static magnetic field (B_0) was produced through the main coil, a 300-kg winding of 16 American wire gauge heavily enameled copper wire. The bobbin was made from 300-series stainless steel; the winding was 81-cm long and had an interior diameter of 40.6 cm. Twenty-six electrically independent layers of wire wound with the same helicity created neat, closely packed coils. The layers were wired as thirteen units in parallel, each unit composed of two layers in series. This winding was operated at 26 A with

a warm voltage drop of 50 V, corresponding to 2.0 A in each wire. The series-parallel configuration was selected to provide an appropriate load to the power supply; however, this configuration provided an additional benefit of having most layer-to-layer voltages being near zero.

To improve magnetic field spatial homogeneity, end-correction windings were also included in this design (Figure 4). Each end-winding was 13 layers with a total vertical length of 17 cm. The magnetic field was calculated along the solenoid symmetry axis by Biot-Savart methods, and the length and number of turns of the end correction windings were chosen to eliminate the second and fourth axial derivatives at the center of the imaging volume. The resulting electromagnet is a so-called “sixth-order” design where the first nonvanishing axial derivative is the sixth derivative.

Three HP 6032A switching power supplies were used to power the electromagnet in constant-current mode. Two of the power supplies were used in series to power the main magnet solenoid. The third power supply provided power to the end correction coils. The total power of roughly 2 kW appeared as heat in the windings and was removed by circulating coolant oil.

The magnetic field gradient coils sat inside the main solenoid magnet and allowed spatial information to be encoded in the MRI signal. The gradient coils also provided a method to improve the magnetic field uniformity with small linear increases/decreases to the field (B_0) in the X, Y, and Z directions (also called shimming). For this system, the gradient coils followed the design of Suits and Wilken (1989). These coils provided better linearity than a simple Maxwell pair (for Z gradient) and Golay coils (for X and Y gradients) and were made from 18 American wire gauge enameled wire. The transverse gradient coils (X and Y) were positioned on a thick polyethylene sheet with grooves to hold the windings. Epoxy was used to bind the windings into an assembly unit. The eight flat assemblies (four each, for X and Y) were curved to fit onto a 35.56-cm outside diameter polyvinyl chloride tube (PVC); the coils were epoxied in place after z gradient coils were wound directly onto the PVC (Figure 5). All gradient coils were secured by winding the assembly with epoxied nylon webbing. The assembly was housed inside the electromagnet bobbin on a PVC pipe. The coils produced $100 \mu\text{T A}^{-1} \text{ cm}^{-1}$, yielding adequate gradient strengths with currents under 10 A. An active cooling system for the gradient coils was found to be unnecessary.

The RF coils had a quadrature mode transmit/receive RF coil design with X-directed and Y-directed saddle RF coils. Driving the two at a 90° phase difference produces a rotating RF field. Compared to linear polarization, the quadrature design results in a 3 dB improvement in received signal-to-noise ratio (SNR) and a 41% increase in RF field strength (B_1) for a given transmitter power. The coils were wound

FIGURE 2 Low-field magnetic resonance imaging (LF-MRI) Rhizotron electronic components schematic

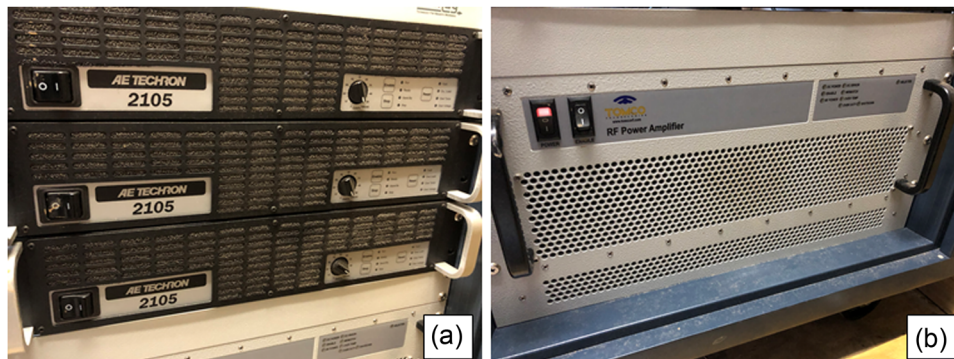
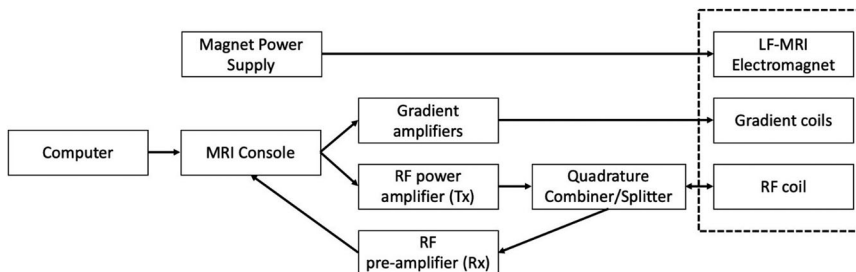


FIGURE 3 Low-field magnetic resonance imaging (LF-MRI) subsystems: X, Y and Z gradient amplifiers (a), and radio frequency amplifier (b)



FIGURE 4 The magnet (left) was constructed on a stainless-steel bobbin, wound with copper wire. The gray plastic polyvinyl chloride (PVC) housing (right) used recirculating oil to cool the magnet

on 28.9 cm outside diameter PVC using 0.635 cm copper refrigeration tubing. Where coils crossed, one was flattened against the PVC (Figure 6) and the other was flattened to the opposite side so that, despite overlapping, the coils were the same diameter. The RF coil was resonated using polyester film capacitors that were hand selected to bring the two coils (X and Y) to the same resonance frequency within 2 kHz. The



FIGURE 5 Gradient coils for the low-field magnetic resonance imaging (LF-MRI) magnet. Z gradient coils were wound directly onto the plastic polyvinyl chloride (PVC) pipe, while X and Y gradient coils were constructed using a form and attached later. The gradient coils are located between the magnet and the radio frequency coil



FIGURE 6 The radio frequency coil was constructed using a quadrature design with X and Y direction saddle coils and was wound on 28.9 cm plastic polyvinyl chloride (PVC) pipe

two saddle coils were constructed and mounted perpendicular to each other to avoid coupling. One turn of each resonant coil was connected to a coaxial driving cable using capacitive coupling.

The oil pump and water chiller were situated close to the magnet and were used in tandem as a cooling system for the electromagnet. The water chiller (CFT-75, Thermo Neslab LLC.) was used to circulate 20 °C tap water using a 0.635-cm diameter copper refrigeration tubing wound around the electromagnet and resting in hydraulic fluid. Hydraulic fluid was used as a cooling oil and was circulated around the main and end windings of the electromagnet via the oil pump. With this design, we did not have any noticeable temperature increase of the sample above what was normal from being outside on a sunny day.

A quadrature combiner/splitter was used to drive the quadrature RF coils. The combiner/splitter was constructed in-house from lumped inductors and capacitors (Figure 7) and placed in-line between the Redstone console and the RF coils.

2.3 | LF-MRI magnet lift system

Two considerations during the design phase for the LF-MRI Rhizotron were the size and mobility of the electromagnet unit in the field. The operating weight of the electromagnet assembly (electromagnet coil, RF coil, Gradient coil, and coolant) was approximately 453.6 kg. For mobility, a lift system was

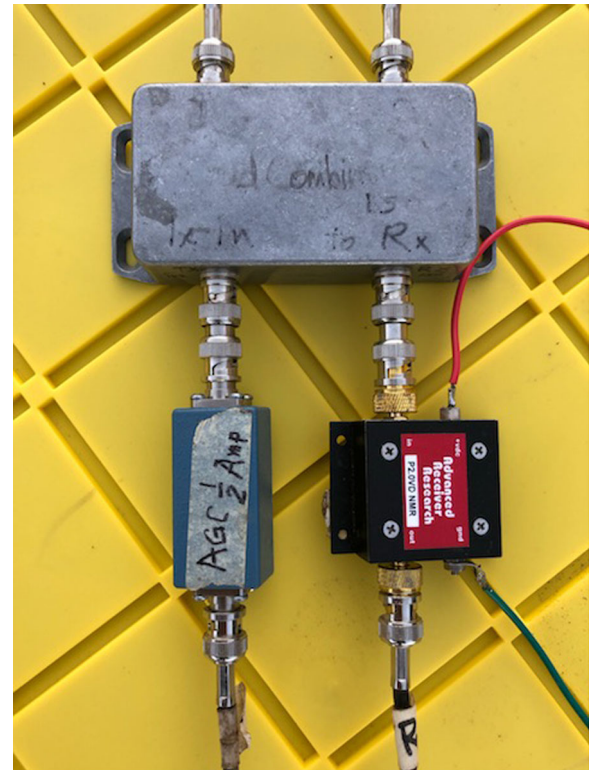


FIGURE 7 Combiner/splitter used to drive the quadrature radio frequency coils

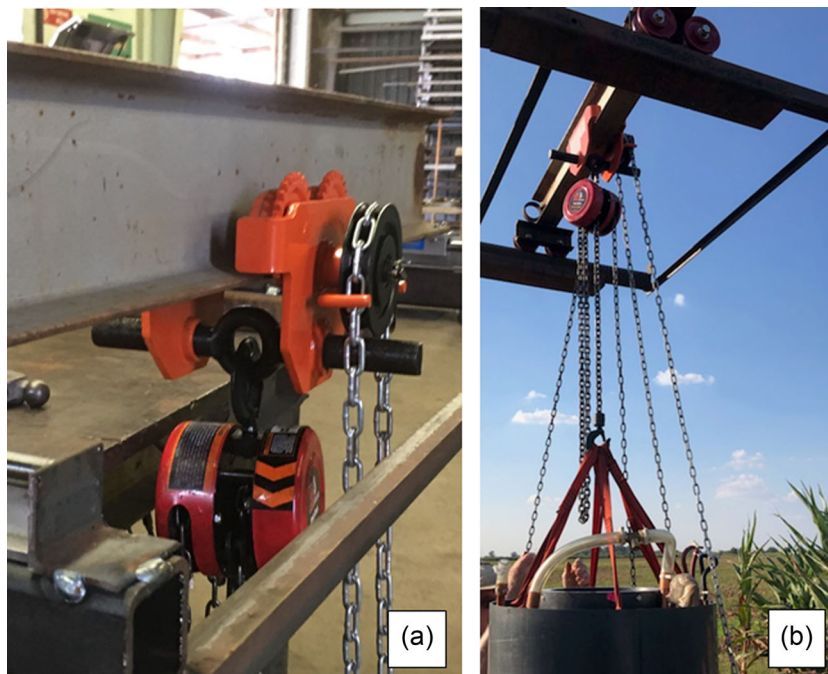
designed to safely lift and move the electromagnet assembly around an experimental site, and to precisely position the assembly as needed.

Two 92-cm long, 0.635-cm right angle guide rails were welded to steel rectangular tubing. The rails supported a 101-cm long I-beam laid perpendicular to the guide rails and rested upon four 10-cm cast iron v-groove wheels, mounted at either end of the I-beam (Figure 8). A tractor with a front-end loader system fitted with forks was used as the platform for the lift system; the forks were used to slide into the rectangular frames supporting the guide rails. A one-ton I-beam walker was fitted on the lower flange of the I beam (Figure 8a). The walker enabled the suspended electromagnet assembly to be moved left or right for precise positioning of the electromagnet above the annular hole. In addition, a one-ton chain hoist was attached to the I-beam walker to allow the electromagnet assembly to be raised and lowered. The chain hoist was secured to the electromagnet assembly by connecting eight nylon lifting straps from the assembly to the end of the chain hoist (Figure 8b).

2.4 | Field data collection

Field data was collected at the Texas A&M AgriLife Research Field Laboratory in Burleson County, TX. Energy sorghum

FIGURE 8 (a) The magnetic resonance imaging (MRI) lift system utilized a chain hoist mounted on an I-beam walker. (b) The I-beam was mounted on a set of rollers. This allowed the lift system to place the MRI anywhere inside a 0.8 m² area



hybrid TX08001, *Sorghum bicolor* (L. Moench) was planted with a row spacing of 76 cm in two soil types: (a) Weswood silt loam, a Udifluventic Haplustept with 25% clay and mixed mineralogy and (b) Belk clay, an Entic Hapludert with 49% clay and mixed mineralogy. The plot sizes were 32 rows, each 30 m long. At time of planting, a solution of liquid ammonium polyphosphate (11-37-0), UAN 32%, and zinc sulfate was applied at seed depth and 5 cm to the side of the seed to yield 45-63-0 +5 Zn (kg ha⁻¹). The plots were sown with enough seed to allow for thinning at 21 d after emergence to 15 cm in-row plant spacing. Seeds were treated with Concep III herbicide protectant, Nugro insecticide, and Apron X fungicide. The plots were grown with natural rainfall totaling 221 mm over the growing season. Root scans were collected at approximately 100 d after emergence. The experimental phase of this work started in August 2019 (approximately 15 d after planting), with 2-D images collected in late November 2019, and 3-D data collected in October 2020. Twelve cores were collected for the 2-D data, with six cores collected in the Weswood silt loam soil and six cores collected in the Belk clay soil type. The 3-D data was collected in a similar manner in the Belk clay soil. The time span for in-field measurement allowed the system to be tested under a range of peak daytime temperatures (0.5–37.8 °C), along with typical humidity, dust, and rain associated with field conditions.

The LF-MRI Rhizotron can either be placed in-ground centered on a plant, or a core can be extracted and imaged above ground. However, the data presented here were collected with the electromagnet assembly placed on the ground and a 25.4 cm diameter by 28 cm tall core was collected and placed in the imaging zone. A 25.4 cm diameter PVC pipe was pushed into the soil while centered on a sorghum

plant. A hydraulic soil probe (Giddings Machine Company, Inc.) mounted on a one-ton dual axle truck was used to push the PVC into the soil. The truck was anchored into the ground with two 20.32-cm diameter land screws measuring 182.88 cm in length. The PVC plus soil core was excavated and placed in the electromagnet assembly for imaging.

2.5 | Imaging sequence

Imaging data was acquired to visualize root architecture using two MRI sequences. The first approach acquired a series of 2-D projection images, and the second approach was a 3-D sequence. For the 2-D imaging approach, frontal viewing of the projection contained the same information as a rear viewing of the sample even though the images were inverted by 180°. Therefore, it was only necessary to acquire images over 180° of rotation and then calculate the remaining images by image inversion. A series of eight projections were acquired at different angles, each rotated 22.5° from the previous. The eight projections were inverted, and the resulting 16 projections could be played sequentially to create an animation displaying 3-D architecture of the root system. The acquisition time for the eight projections was 2 h 16 min. Each image matrix was 128 × 128 pixels with a field of view (FOV) of 28 cm × 28 cm, or 2.2 mm pixel⁻¹.

For a given MRI data set, progressing from a 2-D to a 3-D image provided more complete information about root architecture, but also significantly increased the acquisition time due to the independent phase encoding in two dimensions. MRI involves scanning over k-space, with the number of values to be acquired equaling the number of voxels (volume

elements) in the final image. A 3-D image has many more voxels than a 2-D projection, so it has more k-values and requires more time to acquire. In this work, an acquisition time of 13 h yielded a 3-D image reconstructed to $128 \times 128 \times 128$ pixels with FOV of $28 \text{ cm} \times 28 \text{ cm} \times 28 \text{ cm}$, or $2.2 \times 2.2 \times 2.2 \text{ mm}$ voxels.

An MRI imaging spin echo sequence with CPMG (Carr-Purcell-Meiboom-Gill) (Slichter, 1990) timing was used. Sixteen echoes were acquired and summed to improve the low SNR. An 8 ms pulse spacing (τ) allowed for acquisition of signal from root water, while excluding signal from soil water. A dwell time of $32 \mu\text{s}$ was used with a repetition time of 600 ms for the 2-D sequence while a repetition time of 970 ms was used for the 3-D sequence. Further details of the sequences used here have been published in previous work (Bagnall et al., 2020).

The program NMRrooting (Pflugfelder & Dusschoten, 2020), is an open source python program used to analyze the imaging data obtained from the LF MRI system. The program creates an image segmentation, which is then used to calculate all other root metrics.

3 | RESULTS AND DISCUSSION

The 2-D root structure projection images collected using the LF-MRI Rhizotron in the above ground configuration are shown in Figure 9. The approximate acquisition time for one image was 16.5 min. Eight projections were needed to create a 360-degree view of the root system architecture which took approximately 2 h 16 min. Figures 9a and 9b show samples # 4 and #6 from the Weswood soil collected during the 2019 field season. Figures 9c and 9d show sorghum roots in the Belk and from samples #8 and #10, respectively, also collected in 2019. In all cases, the displayed image is the first in a series of eight projection images. The FOV for these images is 280 mm, with an original image matrix of 128×128 . The image matrix was then zero filled to create a matrix of size 256×256 , as displayed, using the same process described in Bagnall et al. (2020). These 2-D images demonstrate root architecture with a relatively short data acquisition window. Currently however, quantitative data mining from this type of data is difficult, labor intensive, and would require much larger data sets than we produced here. Since 2-D images have less information than a 3-D data set, a 3D imaging sequence was implemented.

In the 2020 planting season, a new 3-D image sequence was designed to address the image analysis difficulties found with the 2-D projection data. The 3-D image sequence required a 13-hr acquisition time for each plant, with a matrix size of $128 \times 128 \times 128$ and a voxel size of 2.2 mm. Figure 10 shows a side view slice and a top view slice from a 3-D data set collected from a sorghum plant grown in Belk clay. Data collec-

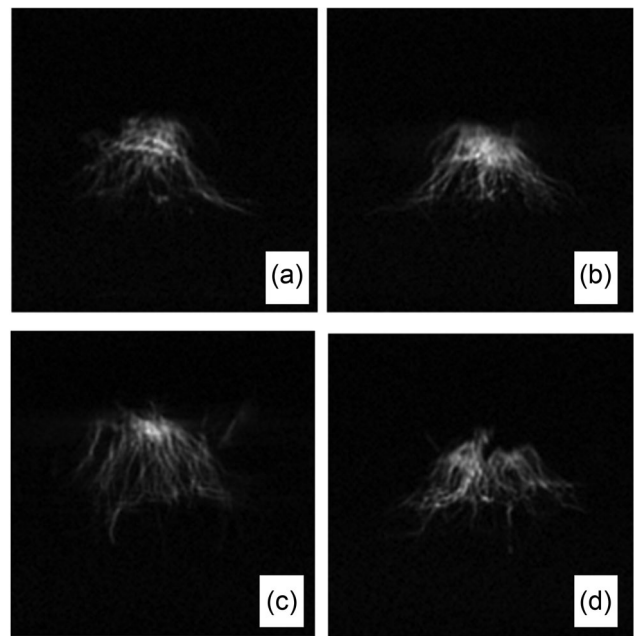


FIGURE 9 2-D image projections of sorghum roots. This image has an in-plane resolution of 2.2 mm, and each image takes approximately 16 minutes to complete. (a) Weswood sample #4. (b) Weswood sample # 6. (c) Belk sample #8. (d) Belk sample #10. The FOV for these images are 280 mm, with an original matrix size of 128×128 . For better visualization, a 256×256 zero-filled interpolation of the root data were carried out and the images are displayed here

tion in a 3-D format enabled the use of NMRrooting software to provide preliminary characterization of root traits.

The NMRrooting software is an open-source Python package, which can calculate root metrics from segmentation of the image data. Figure 11 shows a root image with the segmentation overlaid on the image as colored lines. In this case, data resolution is somewhat low, in part because of operation at very low magnetic field and consequently relatively low SNR, resulting in only the nodal roots being seen. As can be seen in Figure 11, the program has difficulty with the segmentation and can overestimate root length. This is probably due to being written for a high-field MRI system and would need to be adjusted to fit the output of the specific MRI system it is being applied to.

4 | CONCLUSIONS

We have detailed in this work the design and deployment of a LF-MRI Rhizotron that is suitable for in-field scanning in an outdoor agricultural setting. This work is the first step in the development of a truly mobile in-ground field-based LF-MRI system. The low-field system allows the MRI to be unperturbed by operation in high clay soils and is capable of

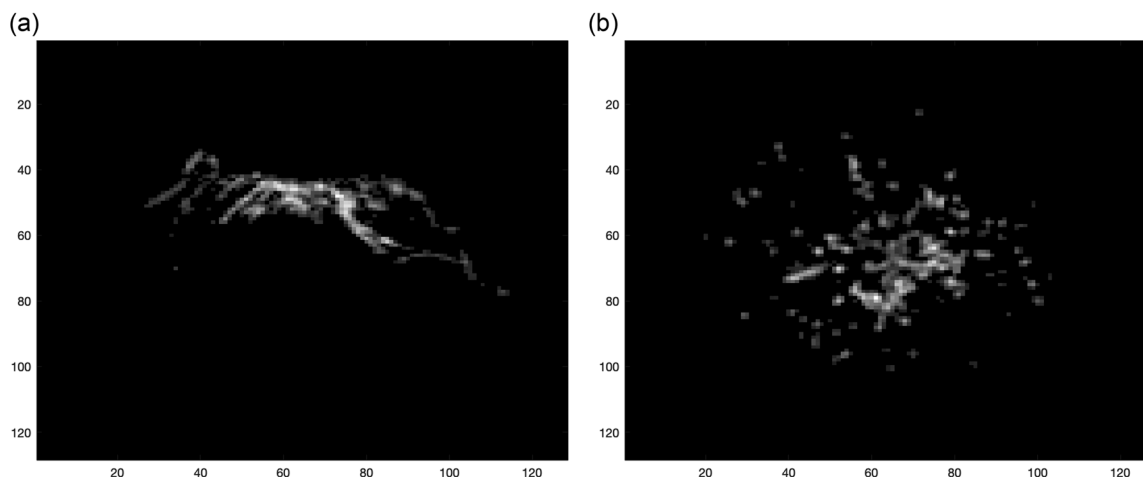


FIGURE 10 Side view (a) and top view (b) slice from the low-field magnetic resonance imaging (LF-MRI) 3-D image set collected from a sorghum plant grown under field conditions in a Belk clay soil in the summer of 2020

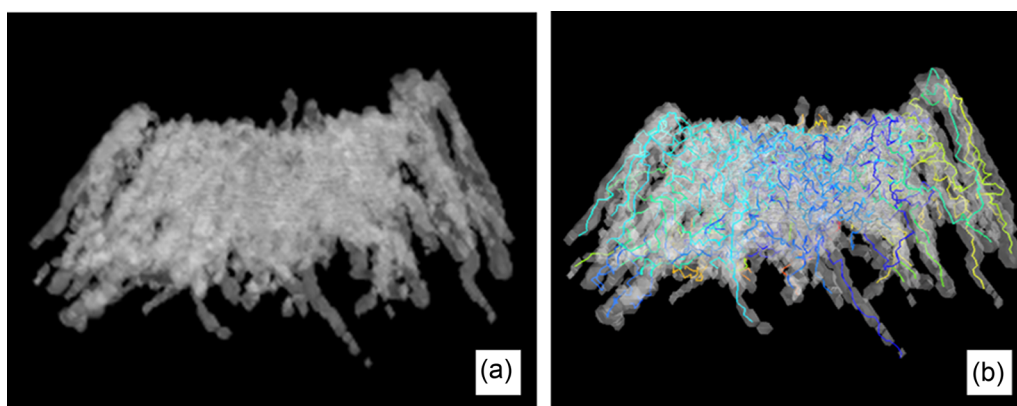


FIGURE 11 Segmentation of roots magnetic resonance imaging (MRI) using the NMRrooting program. (a) The original image projection from the 3-D data set. (b) The program tries to separate out and map each root, the colors represent different nodal roots and is generated by the segmentation process

acquiring root data in the field either by pulling large cores and imaging them above ground or by excavation and imaging in situ. The system is light enough to be moved around the field using a tractor and operates with two portable ac power generators.

In using the ex situ field method, we were able to produce 2-D projection images with relatively short acquisition times that showed root architecture. With longer acquisition times, we acquired a 3-D data set. The NMRrooting software provides a good starting point for processing MRI data sets of roots but it needs to be adjusted for the specific MRI system it is being used with.

The work presented here demonstrates that low-field magnetic resonance systems can work well for imaging roots in high clay soils under field conditions; however, the data produced by this system also indicate that the 2 MHz value (47 mT), from a practical standpoint, is at the low end of the

usable range for root phenotyping. While we were able to collect root imaging data, the resolution was relatively coarse. Likewise, the time scale required to collect data in the 3D format is very long (13 h). From a user perspective, the system is comparatively simple to set up and operate and works without imaging artifact in high clay structured and unstructured soils. We conclude that a higher magnetic field strength system that still falls within the low-field range would produce even better data and is the next step in producing a practical and useful field based LF-MRI Rhizotron.

AUTHOR CONTRIBUTIONS

G. Cody Bagnall: Formal Analysis, Fabrication, Investigation, Methodology, Resources, Software, Validation, Visualization, Writing-original draft. Stephen A. Altobelli, Conceptualization, Investigation, Writing-original draft, Methodology, Formal Analysis, Software, Validation, Visualization. Mark

S. Conradi: Conceptualization, Fabrication, Investigation, Writing-original draft, Methodology, Formal Analysis, Validation, Supervision. Hilary T. Fabich: Conceptualization, Investigation, Writing-original draft, Methodology, Formal Analysis, Software, Validation, Visualization, Supervision. Eiichi Fukushima: Conceptualization, Writing-original draft, Methodology, Funding Acquisition. Neha Koonjoo: Investigation, Writing-original draft, Methodology, Formal Analysis, Software, Validation, Visualization. Dean O. Kuethe: Conceptualization, Fabrication, Software, Investigation, Writing-original draft, Methodology, Formal Analysis. William L. Rooney: Conceptualization, Methodology. Karl F. Stupic: Conceptualization, Investigation, Methodology. Bragi Sveinsson: Investigation, Writing-original draft, Methodology, Formal Analysis, Software, Validation, Visualization. Brock Weers: Investigation, Writing-original draft, Methodology, Formal Analysis. Nithya Rajan: Writing-original draft, Supervision, Project Administration. Matthew S. Rosen: Conceptualization, Supervision, Writing-original draft, Funding Acquisition, Methodology. Cristine L. S. Morgan: Conceptualization, Supervision, Writing-original draft, Funding Acquisition, Project Administration.

ACKNOWLEDGMENTS

The information, data, or work presented herein was funded in part by the Advanced Research Projects Agency-Energy (ARPA-E), U.S. Department of Energy, under Award Number DE-AR0000823. The views and opinions of authors expressed herein do not necessarily state or reflect those of the United States Government or any agency thereof.

CONFLICT OF INTEREST

Matt S. Rosen is a co-founder of Hyperfine, Inc., and Intact Data Services, Inc. Cristine L. S. Morgan is a co-founder of Intact Data Services. ABQMR Inc. (including Stephen A. Altobelli, Mark S. Conradi, Hilary T. Fabich, and Eiichi Fukushima) is a co-founder of Intact Data Services.

ORCID

G. Cody Bagnall  <https://orcid.org/0000-0002-8795-0417>

William L. Rooney  <https://orcid.org/0000-0001-7953-1856>

Nithya Rajan  <https://orcid.org/0000-0003-3798-2629>

Matthew S. Rosen  <https://orcid.org/0000-0002-7194-002X>

Cristine L. S. Morgan  <https://orcid.org/0000-0001-9836-0669>

REFERENCES

Araújo, A. P., Fernandes, A. M., Kubota, F. Y., Brasil, F. C., & Teixeira, M. G. (2004). Sample size for measurement of root traits on common

- bean by image analysis. *Pesquisa Agropecuaria Brasileira*, 39, 313–318. <https://doi.org/10.1590/S0100-204X2004000400003>
- Ayalew, H., Ma, X., & Yan, G. (2015). Screening wheat (*Triticum* spp.) genotypes for root length under contrasting water regimes: Potential sources of variability for drought resistance breeding. *Journal of Agronomy and Crop Science*, 201, 189–194. <https://doi.org/10.1111/jac.12116>
- Bagnall, G. C., Koonjoo, N., Altobelli, S. A., Conradi, M. S., Fukushima, E., Kuethe, D. O., Mullet, J. E., Neely, H., Rooney, W. L., Stupic, K. F., Weers, B., Zhu, B. O., Rosen, M. S., & Morgan, C. L. S. (2020). Low-field magnetic resonance imaging of roots in intact clayey and silty soils. *Geoderma*, 370. <https://doi.org/10.1016/j.geoderma.2020.114356>
- Borisjuk, L., Rolletschek, H., & Neuberger, T. (2012). Surveying the plants world by magnetic resonance imaging. *The Plant Journal*, 70, 129–146. <https://doi.org/10.1111/j.1365-313X.2012.04927.x>
- Bucksch, A., Burrige, J., York, L. M., Das, A., Nord, E., Weitz, J. S., & Lynch, J. P. (2014). Image based high-throughput field phenotyping of crop roots. *Plant Physiology*, 166(2), 470–486. <https://doi.org/10.1007/BF02187258>
- Chloupek, O. (1997). Evaluation of the size of a plants root system using its electrical capacitance. *Plant and Soil*, 48(2), 525–532. <https://doi.org/10.1007/BF02187258>
- Fenta, B., Beebe, S., Kunert, K., Burrige, J., Barlow, K., Lynch, J., & Foyer, C. (2014). Field phenotyping of soybean roots for drought stress tolerance. *Agronomy*, 4(3), 418–435. <https://doi.org/10.3390/agronomy4030418>
- Fiorani, F., & Schurr, U. (2013). Future Scenarios for Plant Phenotyping. *Annual Review of Plant Biology*, 64, 267–291. <https://doi.org/10.1146/annurev-arplant-050312-120137>
- Garnett, T., Conn, V., & Kaiser, B. N. (2009). Root based approaches to improving nitrogen use efficiency in plants. *Plant, Cell and Environment*, 32(9), 1272–1282. <https://doi.org/10.1111/j.1365-3040.2009.02011.x>
- Grift, T. E., Novais, J., & Bohn, M. (2011). High-Throughput phenotyping technology for maize roots. *Biosystems Engineering*, 110, 40–48. <https://doi.org/10.1016/j.biosystemseng.2011.06.004>
- Gruwel, M. L. H. (2014). In Situ magnetic resonance imaging of plant roots. *Vadose Zone Journal*, 13(3), 1–8. <https://doi.org/10.2136/vzj2013.08.0158>
- Hall, L. D., Gao Amin, M. H., Dougherty, E., Sanda, M., Votrubova, J., Richards, K. S., Chorley, R. J., & Cislserova, M. (1997). MR properties of water in saturated soils and resulting loss of MRI signal in water content detection at 2 tesla. *Geoderma*, 80, 431–448. [https://doi.org/10.1016/S0016-7061\(97\)00065-7](https://doi.org/10.1016/S0016-7061(97)00065-7)
- Henry, A., Gowda, V. R. P., Torres, R. O., McNally, K. L., & Serraj, R. (2011). Variation in root system architecture and drought response in rice (*Oryza Sativa*): Phenotypin of the Oryza SNP panel in rainfed lowland fields. *Field Crops Research*, 120, 205–214. <https://doi.org/10.1016/j.fcr.2010.10.003>
- Hillnhutter, C., Sikora, R. A., Oerke, E.-C., & Van Dusschoten, D. (2012). Nuclear magnetic resonance: A tool for imaging belowground damage caused by heterodera schachtii and rhizoctonia solani on sugar beet. *Journal of Experimental Botany*, 63(1), 319–327. <https://doi.org/10.1093/jxb/err273>
- Kano-Nakata, M., Nakamura, T., Mitsuya, S., & Yamauchi, A. (2019). Plasticity in root system architecture of rice genotypes exhibited

- under different soil water distributions in Soil Profile. *Plant Production Science*, 22(4), 501–509. <https://doi.org/10.1080/1343943X.2019.1608836>
- Koevoets, I. T., Venema, J. H., Elzenga, J. T. M., & Testerink, C. (2016). Roots withstanding their environment: Exploiting root system architecture responses to abiotic stress to improve crop tolerance. *Frontiers in Plant Science*, 7, 1355. <https://doi.org/10.3389/fpls.2016.01335>
- Koonjoo, N., Zhu, B., Bagnall, G. C., Bhutto, D., & Rosen, M. S. (2021). Boosting the signal-to-noise of low-field MRI with deep learning image reconstruction. *Scientific Reports*, 8248(2021). <https://doi.org/10.1038/s41598-021-87482-7>
- Logsdon, S. D. (2009). CS616 Calibration: Field versus Laboratory. *Soil Science Society of America Journal*, 73(1), 1–6. <https://doi.org/10.2136/sssaj2008.0146>
- López-Bucio, J., Cruz-Ramírez, A., & Herrera-Estrella, L. (2003). The Role of nutrient availability in regulating root architecture. *Current Opinion in Plant Biology*, 6(3), 280–287. [https://doi.org/10.1016/S1369-5266\(03\)00035-9](https://doi.org/10.1016/S1369-5266(03)00035-9)
- Ma, L., Shi, Y., Siemianowski, O., Yuan, B., Egener, T. K., Mirnezami, S. V., Lind, K. R., Ganapathysubramanian, B., Venditti, V., & Cademartiri, L. (2019). Hydrogel-based transparent soils for root phenotyping in vivo. *Proceedings of the National Academy of Sciences of the United States of America*, 116(22), 1103–11068. <https://doi.org/10.1073/pnas.1820334116>
- Mairhofer, S., Zappala, S., Tracy, S., Sturrock, C., Bennett, M. J., Mooney, S. J., & Pridmore, T. P. (2013). Recovering complete plant root system architectures from soil via X-ray μ computed tomography. *Plant Methods*, 9, 8. <https://doi.org/10.1186/1746-4811-9-8>
- Messmer, R., Fracheboud, Y., Bänziger, M., Stamp, P., & Ribaut, J.-M. (2012). Advancing the use of minirhizotrons in wetlands. *Plant and Soil*, 352, 23–39. <https://doi.org/10.1016/j.fcr.2011.06.010>
- Messmer, R., Fracheboud, Y., Bänziger, M., Stamp, P., & Ribaut, J.-M. (2011). Drought stress and tropical maize: QTLs for leaf greenness, plant senescence, and root capacitance. *Field Crops Research*, 124(1), 93–103. <https://doi.org/10.1016/j.fcr.2011.06.010>
- Metzner, R., Eggert, A., Van Dusschoten, D., Pflugfelder, D., Gerth, S., Schurr, U., Uhlmann, N., & Jahnke, S. (2015). Direct comparison of MRI and X-ray CT technologies for 3D imaging of root systems in soil: Potential and challenges for root trait quantification. *Plant Methods*, 11(17), 1–11. <https://doi.org/10.1186/s13007-015-0060-z>
- Miller, T. W., Borchers, B., Hendrickx, J. M., Hong, S., Dekker, L. W., & Ritsema, C. J. (2002). Effects of soil physical properties on GPR for landmine detection. In *Fifth international symposium on technology and the mine problem* (pp. 1–10).
- Mooney, S. J., Pridmore, T. P., Helliwell, J., & Bennett, M. J. (2012). Developing X-ray computed tomography to non-invasively image 3-D root systems architecture in soil. *Plant and Soil*, 352, 1–22. <https://doi.org/10.1007/s11104-011-1039-9>
- Paez-Garcia, A., Motes, C., Scheible, W.-R., Chen, R., Blancaflor, E., & Monteros, M. (2015). Root traits and phenotyping strategies for plant improvement. *Plants*, 4, 334–355. <https://doi.org/10.3390/plants4020334>
- Paustian, K., Campbell, N., Dorich, C., Marx, E., & Swan, A. (2016). *Assessment of potential greenhouse gas mitigation from changes to crop root mass and architecture*. ARPA-E ROOTS FOA.
- Pflugfelder, D., Metzner, R., Van Dusschoten, D., Reichel, R., Jahnke, S., & Koller, R. (2017). Non-invasive imaging of plant roots in different soils using magnetic resonance imaging (MRI). *Plant Methods*, 13, 1–9. <https://doi.org/10.1186/s13007-017-0252-9>
- Pflugfelder, D., & Dusschoten, D. V. (2020). The NMRrooting website. https://www.fz-juelich.de/ibg/ibg-2/EN/methods/NMRrooting/nmrooting_node.html
- Pingault, L., Zogli, P., Brooks, J., & Libault, M. (2018). Enhancing phenotyping and molecular analysis of plant root systems using ultrasound aeroponic technology. *Current Protocols in Plant Biology*, 3(4), e20078. <https://doi.org/10.1002/cppb.20078>
- Rogers, H. H., & Bottomley, P. A. (1987). In Situ nuclear magnetic resonance imaging of root: Influence of soil type, ferromagnetic particle content and soil water. *Agronomy Journal*, 79, 957–965. <https://doi.org/10.2134/agronj1987.00021962007900060003x>
- Slichter, C. P. (1990). *Principles of magnetic resonance*. Springer.
- Suits, B. H., & Wilken, D. E. (1989). Improving magnetic field gradient coils for NMR imaging. *Journal of Physic E: Scientific Instrumentation*, 22(8), 565–573. <https://doi.org/10.1088/0022-3735/22/8/007>
- Trachsel, S., Kaeppler, S. M., Brown, K. M., & Lynch, J. P. (2011). Shovelomics: High throughput phenotyping of maize (*Zea Mays* L.) root architecture in the field. *Plant and Soil*, 341, 75–87. <https://doi.org/10.1007/s11104-010-0623-8>
- Van Dusschoten, D., Metzner, R., Kochs, J., Postma, J. A., Pflugfelder, D., Bühler, J., Schurr, U., & Jahnke, S. (2016). Quantitative 3D analysis of plant roots growing in soil using magnetic resonance imaging. *Plant Physiology*, 170, 1176–1188. <https://doi.org/10.1104/pp.15.01388>
- Wasaya, A., Zhang, X., Fang, Q., & Yan, Z. (2018). Root phenotyping for drought tolerance: A review. *Agronomy*, 8, 241–260. <https://doi.org/10.3390/agronomy8110241>
- Wasson, A. P., Rebetzke, G. J., Kirkegaard, J. A., Christopher, J., Richards, R. A., & Watt, M. (2014). Soil coring at multiple field environments can directly quantify variation in deep root traits to select wheat genotypes for breeding. *Journal of Experimental Botany*, 65(21), 6231–6249. <https://doi.org/10.1093/jxb/eru250>
- Zhu, B.o, Liu, J. Z., Cauley, S. F., Rosen, B. R., & Rosen, M. S. (2018). Image reconstruction by domain-transformation manifold learning. *Nature*, 555(7697), 487–492. <https://doi.org/10.1038/nature25988>

How to cite this article: Bagnall, G. C., Altobelli, S. A., Conradi, M. S., Fabich, H. T., Fukushima, E., Koonjoo, N., Kuethe, D. O., Rooney, W. L., Stupic, K. F., Sveinsson, B., Weers, B., Rajan, N., Rosen, M. S., & Morgan, C. L. S. (2022). Design and demonstration of a low-field magnetic resonance imaging rhizotron for in-field imaging of energy sorghum roots. *The Plant Phenome Journal*, 5,e20038. <https://doi.org/10.1002/ppj2.20038>